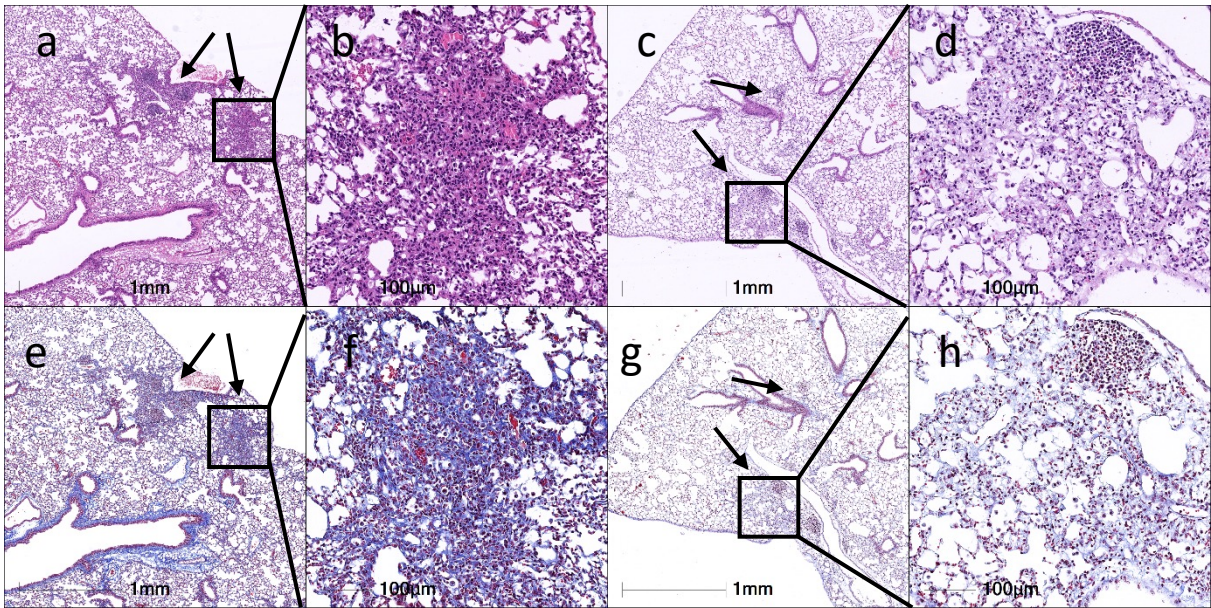
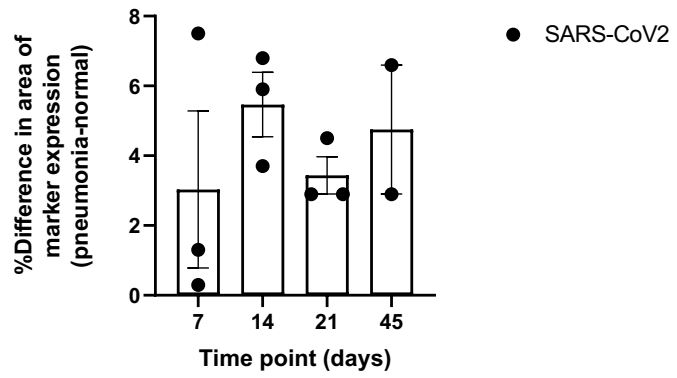


Supplemental Figure 1

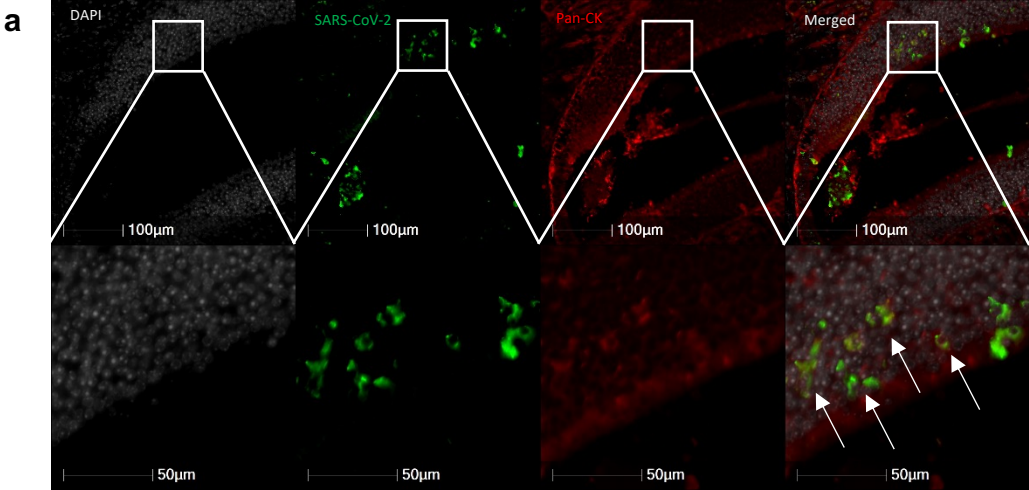


Comparison of Collagen Deposition in Regions of Pneumonia to Normal Lungs

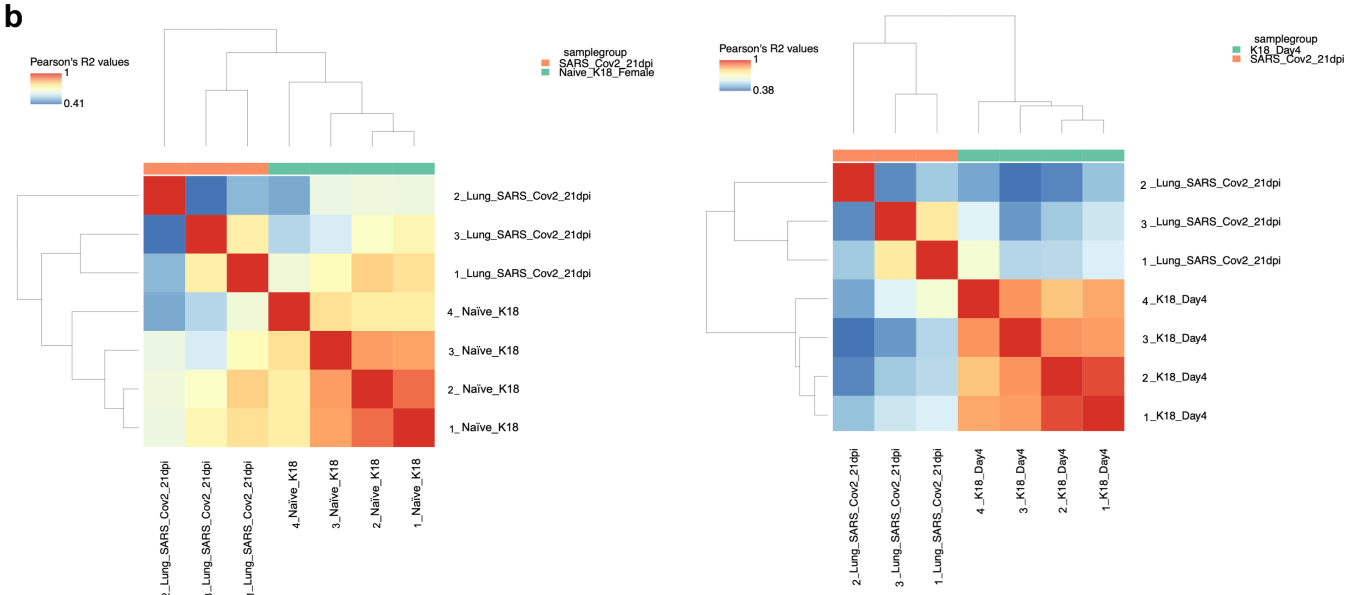


Supplemental Figure 1. Persistent pulmonary pathology in SARS-CoV-2 infected mice out to 45 days post infection (n=2). a-d) At 45 DPI there are persistent, patchy regions of pulmonary consolidation with inflammation (arrows) in SARS-CoV-2 infected mice (a&b Ms 307; c&d Ms 314). e-h) Trichrome staining reveals pulmonary fibrosis without epithelial proliferation in regions of pulmonary consolidation, similar to lesions at 21 DPI.

Supplemental Figure 2

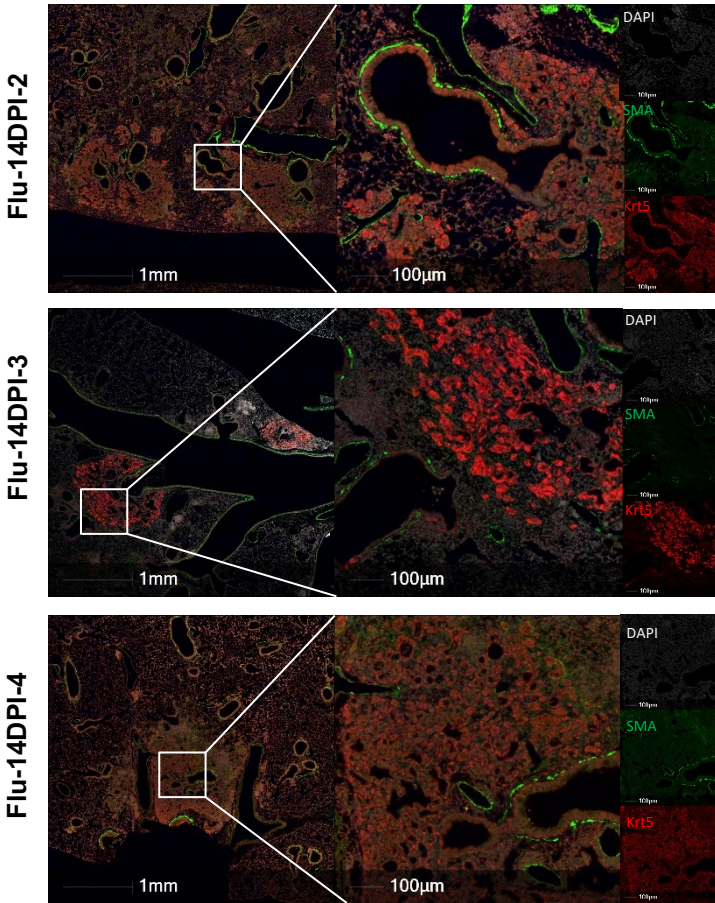


Supplemental Figure 2a. Representative images show SARS-CoV-2 infected respiratory epithelial cells as arrows pointed. (n=1)



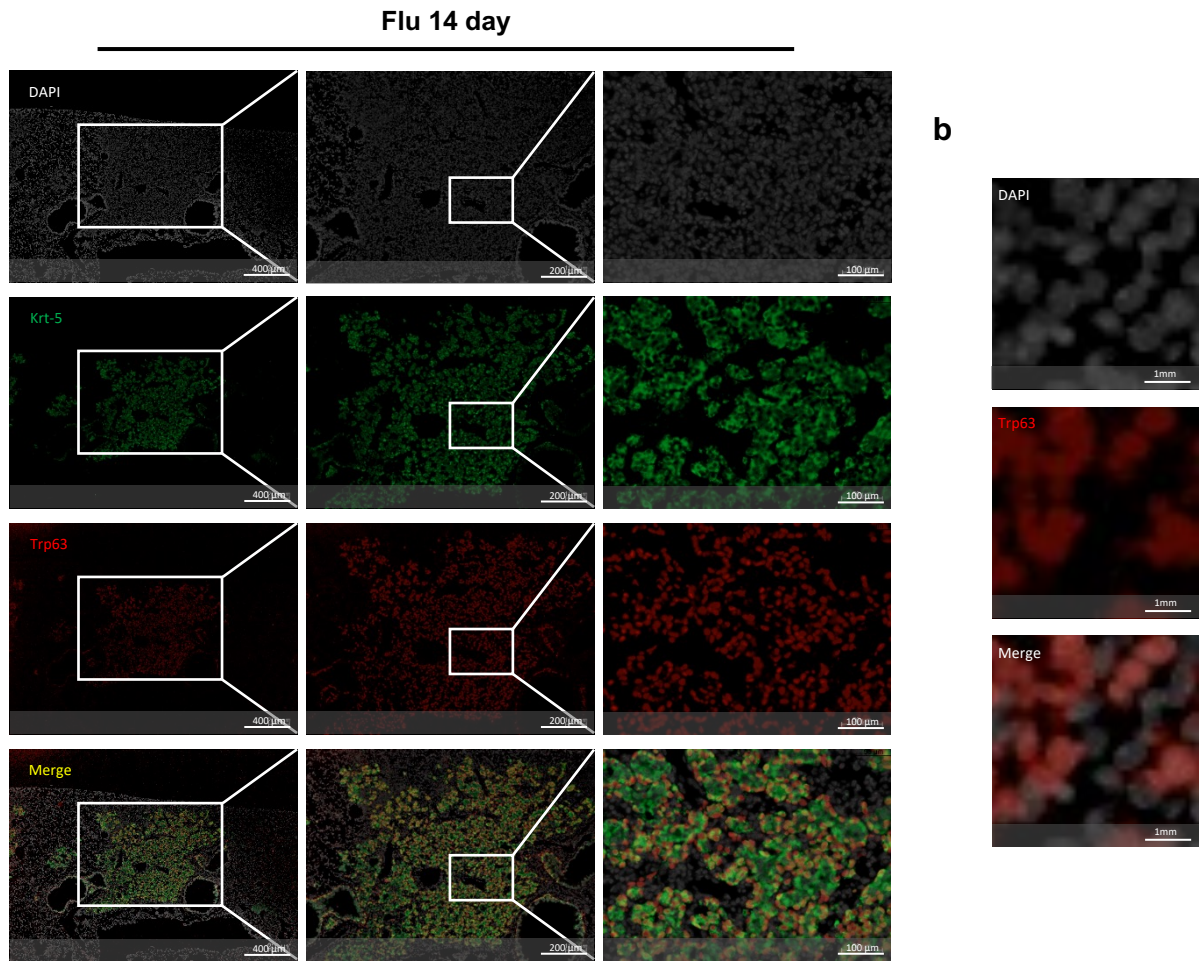
Supplemental Figure 2b. Heatmap to show sample to sample correlation. Two sample groups are presented—SARS CoV2 21 DPI (orange) and Naive K18 and K18 4 DPI (green). Correlations were determined using all genes and a Pearson Correlation Coefficient (PCC). Color indicates PCC with 1 as the darkest red and 0.41 and 0.38 as the darkest blue. Figures represent linear relationship between mice. Representative heatmap for the CoV2 K18 21 DPI and K18 Naive mice (left panel) and CoV2 K18 21 DPI and CoV2 K18 4 DPI mice (right panel).

Supplemental Figure 3



Supplemental Figure 3. Representative images show Krt5+ pod structure in lungs of each of mice infected with sublethal Flu dose at 14 DPI.

Supplemental Figure 4

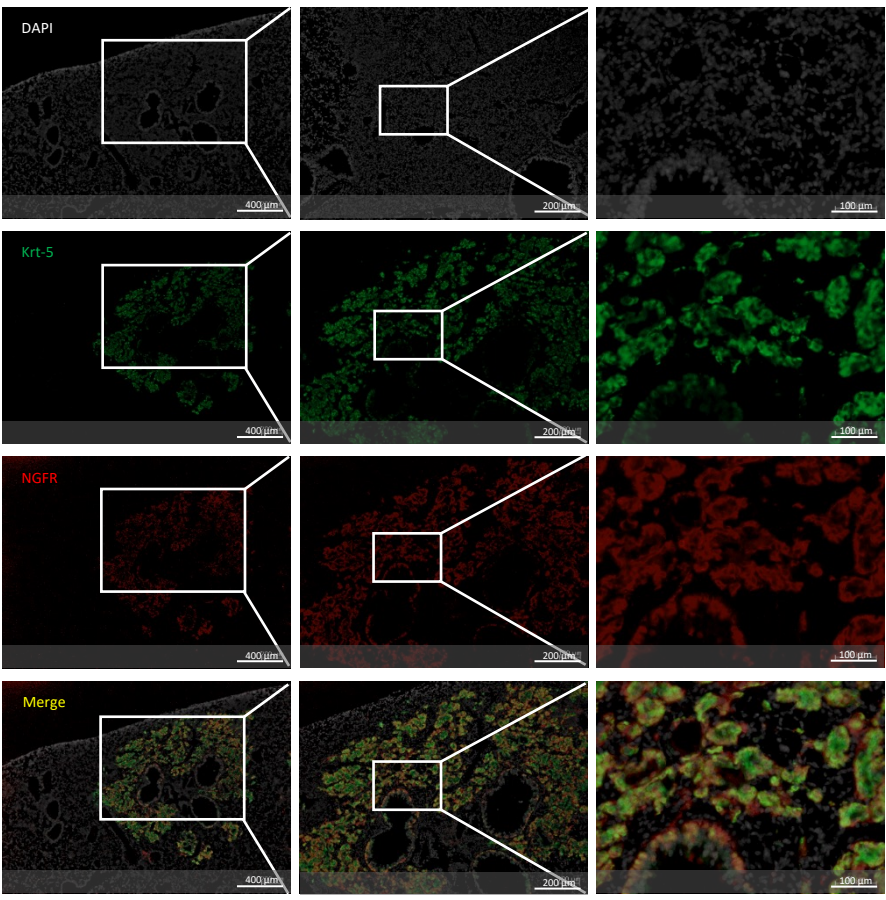


Supplemental Figure 4. Representative image shows the colocalization of Krt-5 and Trp-63 in pulmonary krt5+ “pod” structure of Flu infected mice at 14 DPI.

(a) Lung sections are stained by DAPI (White), Krt-5 (green) and Trp63 (Red). At 14 DPI, Flu infected mouse exhibits Krt5+ “pods” in the lung. The Krt-5 signals colocalize with Trp63 (the highest magnification image in lowest panel). (b) The Trp63 signals colocalize with DAPI.

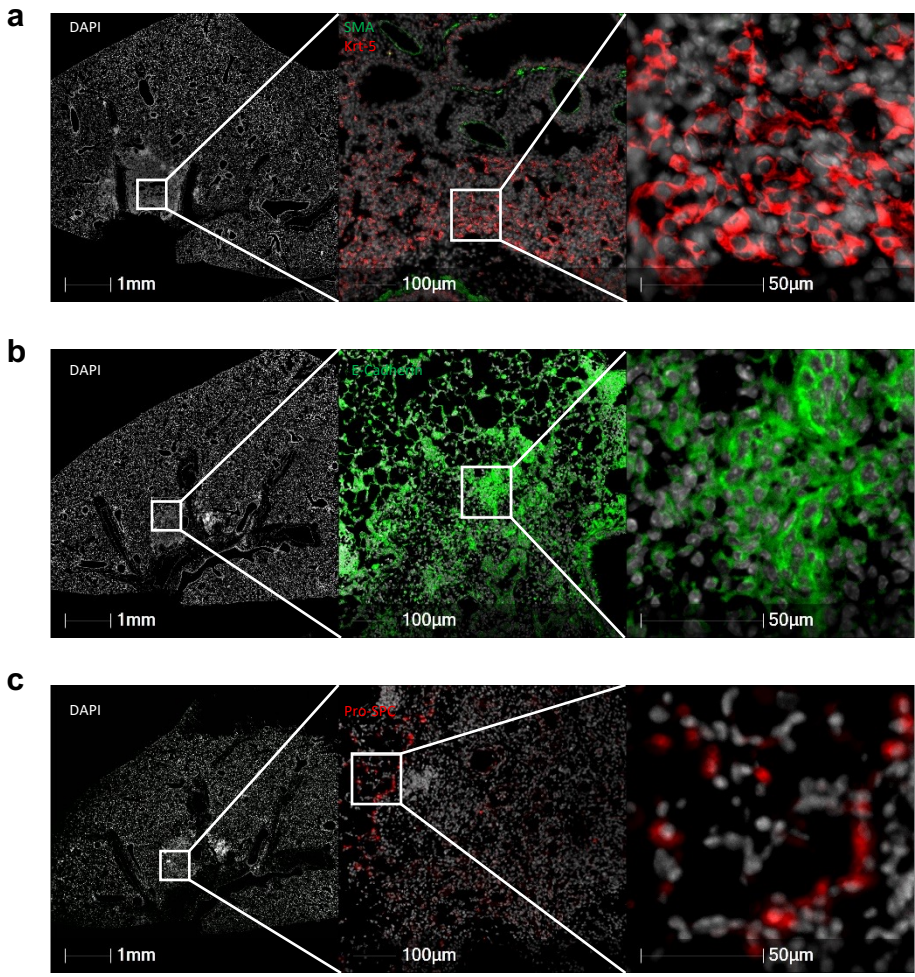
Supplemental Figure 5

Flu 14 day



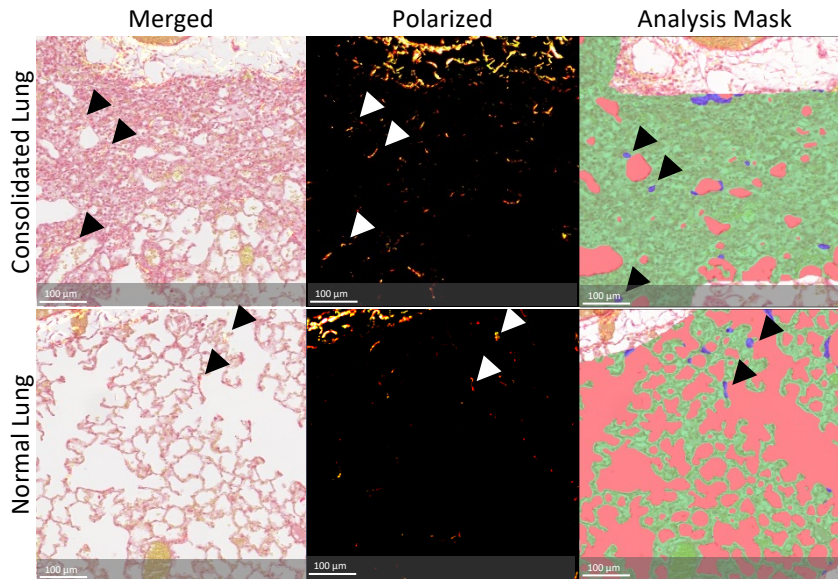
Supplemental Figure 5. Representative image shows the colocalization of Krt-5 and NGFR in pulmonary krt5+ “pod” structure of Flu infected mice at 14 DPI. Lung sections are stained by DAPI (White), Krt-5 (green) and NGFR (Red). At 14 DPI, Flu infected mouse exhibits Krt5+ “pods” in the lung. The Krt-5 signals colocalize with NGFR (the highest magnification image in lowest panel).

Supplemental Figure 6



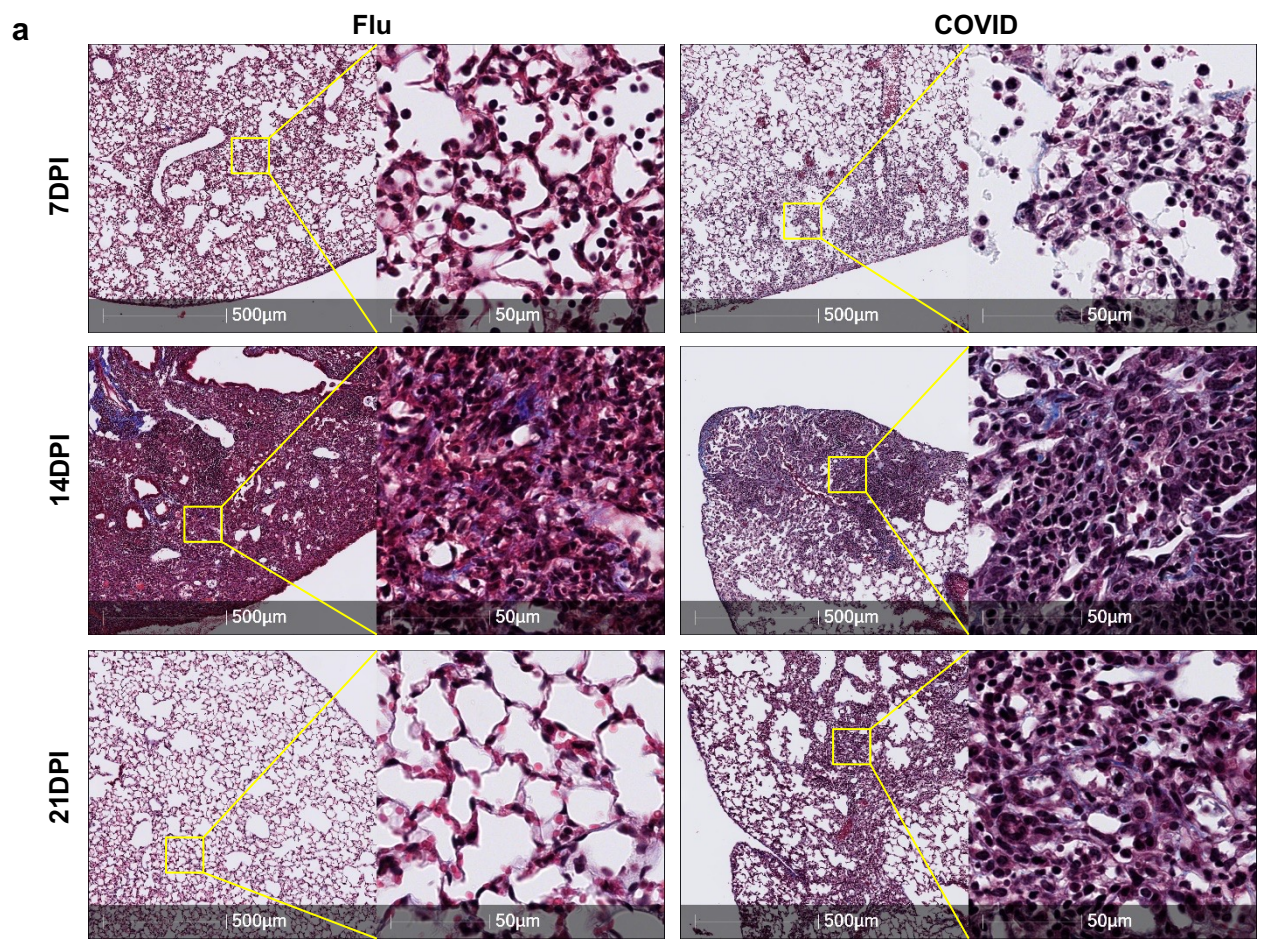
Supplemental Figure 6. Serial sections show the presence of AT1 cells in pulmonary krt-5+ “pod” area and AT2 cells at the edge of pulmonary krt5+ pod area at 14 days post Flu infection (n=4). a-c) Representative images of Krt-5, E-cad, and pro-SPC IF staining. Similar region of lung as determined by DAPI staining. (a) Krt-5+ pod is located by Krt5 fluorescence staining. (b) AT1 cells are stained by E-cad. (c) pro-SPC staining reveals AT2 cells locate at the edge of Krt-5+ pod.

Supplemental Figure 7



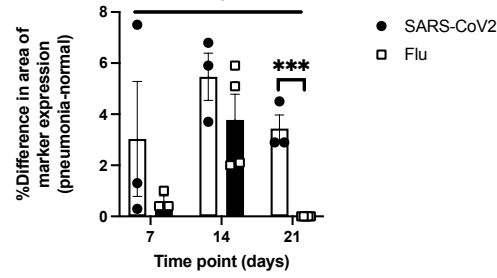
Supplemental Figure 7. Comparison of Fibrosis in Consolidated Lung versus Normal lung in Flu and COVID. Picosirius Red staining for the comparison and quantification of fibrosis in regions of SARS-CoV-2- and Flu-associated pulmonary consolidation. **Left)** PSR staining in combination with polarized light microscopy identifies collagen by red staining and birefringence on merged images (brightfield and polarized, black arrows). **Middle)** Birefringence of collagen (white arrows) is easily seen when viewed with only polarized light and differentiates from background red staining of the merged image. **Right)** Quantification was performed with pattern recognition software trained to recognize the dual expression of red staining and birefringence (blue, black arrows). Regions of interest were drawn to exclude areas of the lung that normally contain collagen within these regions (large vessels and airways). Red = glass, green= Background.

Supplemental Figure 8



b

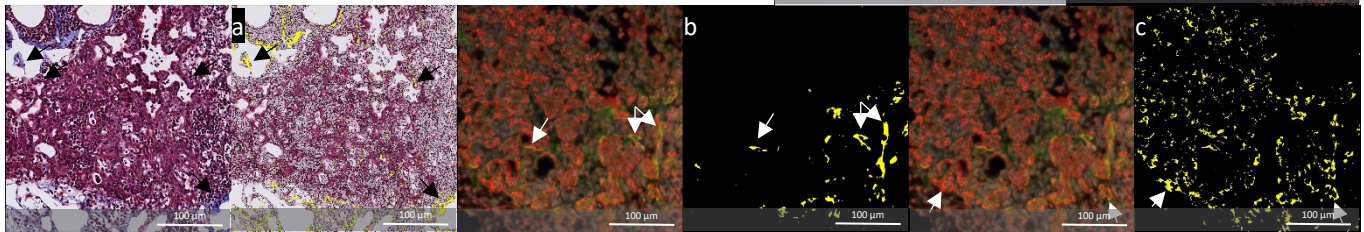
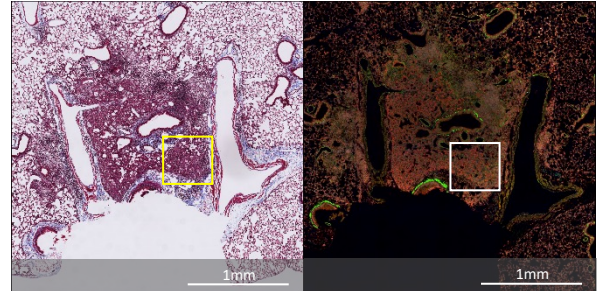
Comparison of Collagen Deposition in Regions of Pneumonia to Normal Lungs



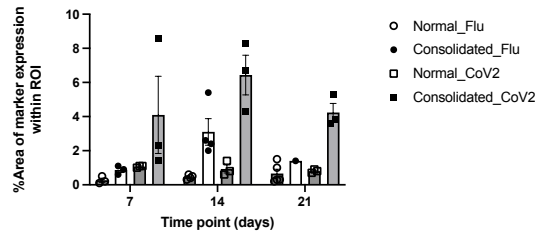
Supplemental Figure 8: Collagen deposited in Flu mouse model and COVID mouse model. (a) Masson's trichrome staining showing collagen deposition in lungs of 1×10^4 TCID₅₀ SARS-CoV-2-infected *K18* mice at 7, 14 and 21 DPI and Flu infected mice at 5, 7, 10 and 14 DPI. **(b)** Comparison of collagen deposition in regions of consolidated lung to normal lung in the same Flu-infected and COVID mice. Data are shown as mean \pm SEM. Two-way analysis of variance (ANOVA) was used to compare collagen deposition level changes over time. One-tailed unpaired Student's t-test was performed to test the difference between two groups at one time point. *** indicates $p < 0.001$.

Supplemental Figure 9

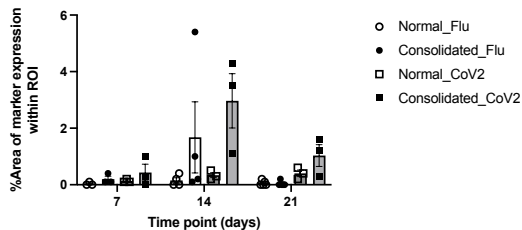
Method of histopathologic quantification of Krt5, smooth muscle actin, and collagen deposition in regions of consolidation. Lung, influenza 14 DPI, region of consolidation. Computer software was used to quantify the deposition of collagen (a, blue), SMA (b, green), or Krt-5 (c, red) in regions of consolidation and normal lung. Detection of each was determined based on intensity of staining in brightfield (collagen) or fluorescence (SMA & Krt-5). The same region of consolidation (box, top right) is used to demonstrate the analysis results for each marker. Arrows highlight foci of marker detection in paired images. Data generated from these analysis for all normal and consolidated regions are shown in graphs below (mean \pm SEM).



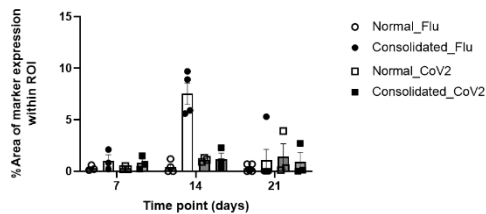
Comparison of Collagen Deposition in Regions of Consolidation to Normal Lungs



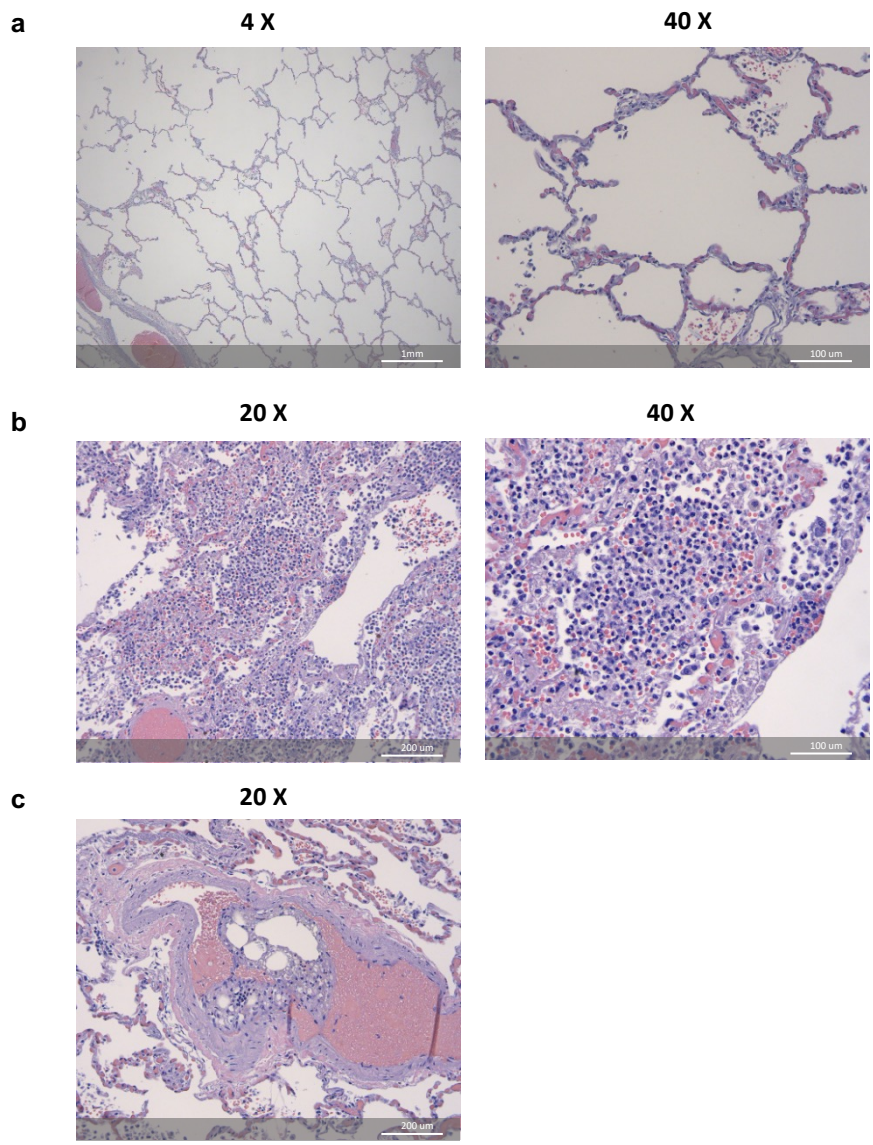
Comparison of SMA expression in Regions of Consolidation to Normal Lungs



Comparison of Krt5 expression in Regions of Consolidation to Normal Lungs



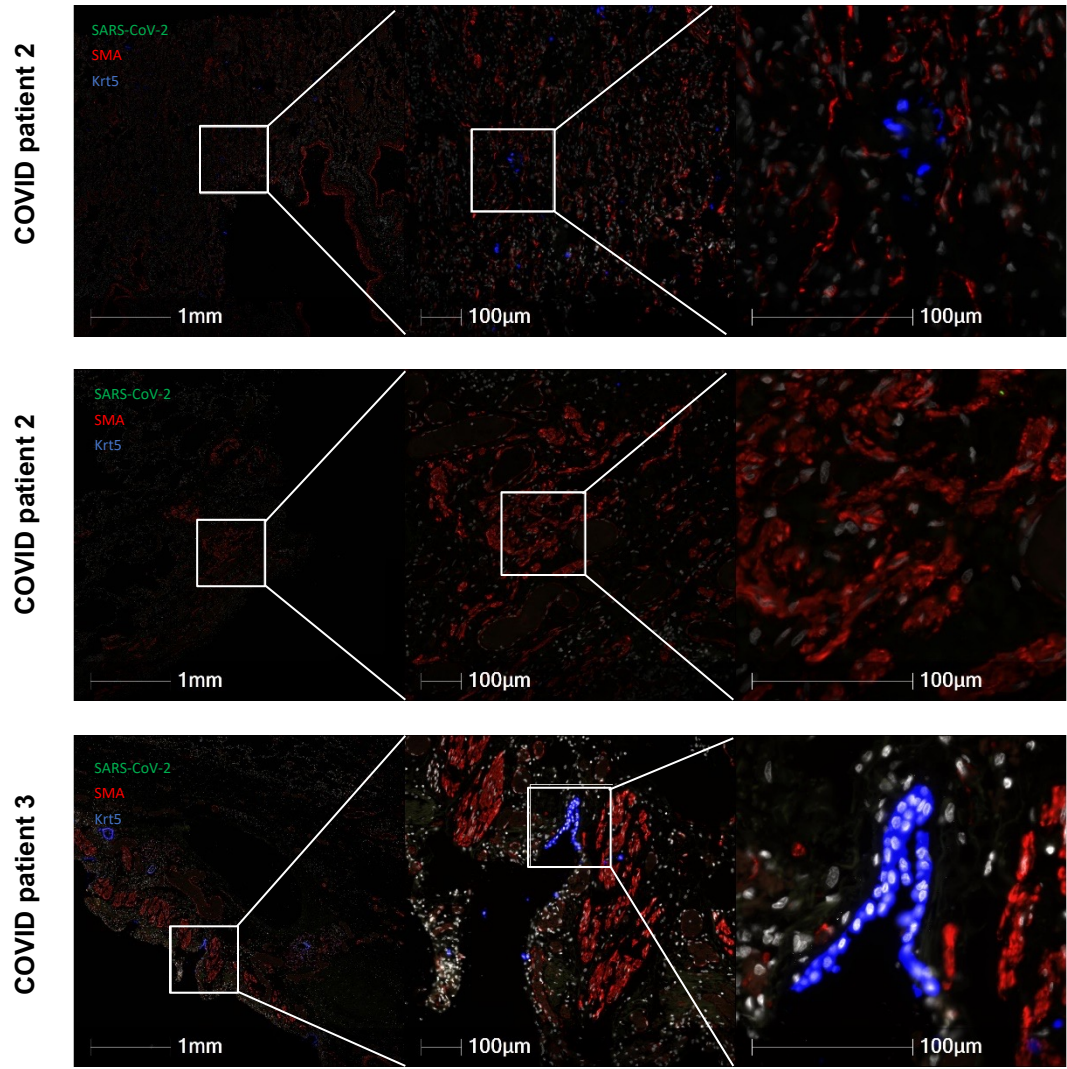
Supplemental Figure 10



Supplemental Figure 10. Representative histopathology of COVID in human patient 3.

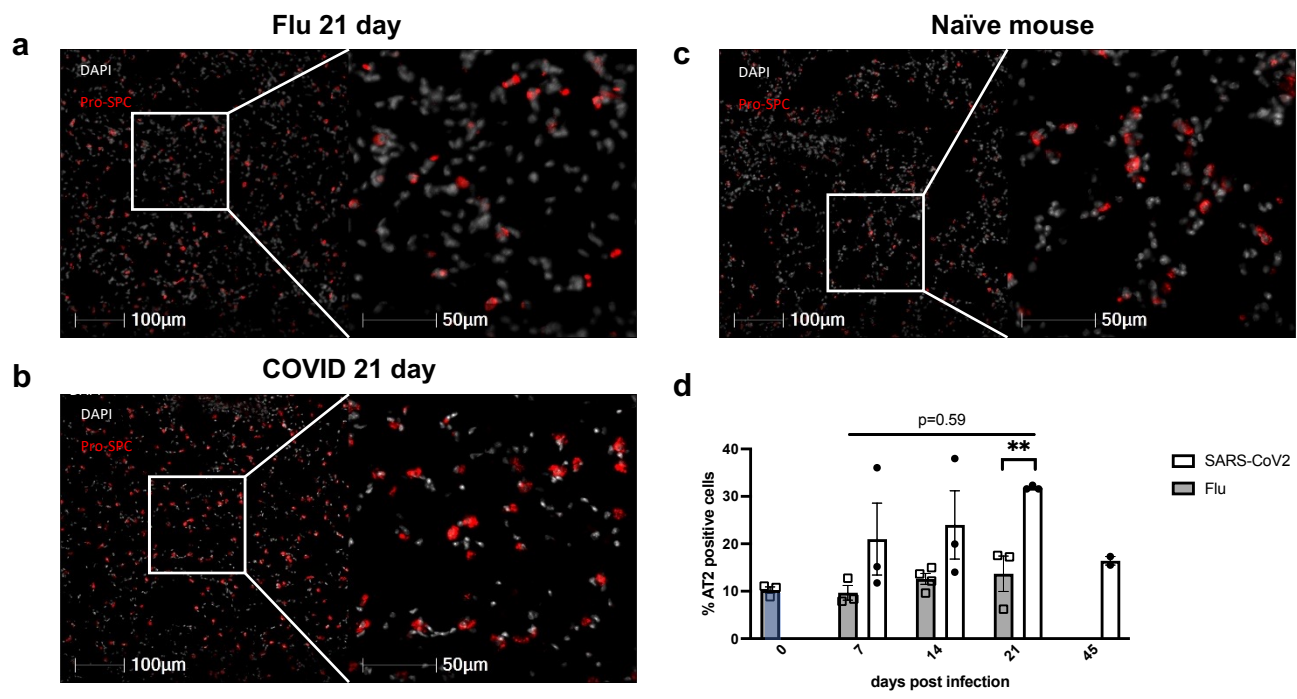
(a) Emphysematous changes characterized by coalescing and expanded alveolar space. (b) Organizing pneumonia with fibrocollagenous aggregates ("Masson bodies") plugging the alveoli. (c) Fat embolus in a small artery.

Supplemental Figure 11



Supplemental Figure 11. No Krt5+ progenitor cell “pod” in COVID human patient 2 and patient 3. Krt5+ cells are only found in the basal layer of airways without any evidence of proliferation.

Supplemental Figure 12



Supplemental Figure 12. Quantification of AT2 cells in the lungs of SARS-CoV-2- and Flu- infected mice. Lung sections are from naïve B6 mice (n = 3), SARS-CoV2-infected z mice at 7 (n = 3) , 14 (n = 3), 21 (n = 3) and 45 (n = 2)DPI, Flu-infected B6 mice at 7 (n = 3) and 14 (n = 4) DPI. a-c) Representative image of AT2 cells in the lung of mice at 21 days post flu infection, 21 days post SARS-COV2 infection and naïve mice respectively. (d) Quantified data for the percentage of AT2 cells among total pulmonary cells in the lung tissue. AT2 cells are counted by Halo software. Mixed-effect analysis is used for flu-SARS comparison. Two-tailed unpaired t test is performed to compare the difference at 21 DPI. ** indicates p < 0.01.

Supplementary Table 1. Mice information

| Strain | Sex | Sample Size | Age/ week | Inoculum | Infection Dose | Time point /DPI | Application |
|---------------|-----------------|-------------|-----------|----------------------|--------------------------------|-----------------|--|
| K18-hACE2 +/- | Male and Female | 3 | 28 | N/A | N/A | 0 | Histology |
| K18-hACE2 +/- | Male | 1 | 16 | SARS-CoV-2(WA1/2020) | 1.0X 10 ⁴ / TCID 50 | 3 | Histology |
| K18-hACE2 +/- | Male and Female | 3 | 6-10 | SARS-CoV-2(WA1/2020) | 2.0X 10 ⁵ / TCID 50 | 7 | Body weight |
| K18-hACE2 +/- | Male and Female | 3 | 12-16 | SARS-CoV-2(WA1/2020) | 1.0X 10 ⁴ / TCID 50 | 7 | Histology |
| K18-hACE2 +/- | Male and Female | 3 | 12-16 | SARS-CoV-2(WA1/2020) | 1.0X 10 ⁴ / TCID 50 | 14 | Histology |
| K18-hACE2 +/- | Male and Female | 3 | 10 | SARS-CoV-2(WA1/2020) | 1.0X 10 ⁴ / TCID 50 | 21 | Body weight/Histology /Viral load/Bulk RNA seq |
| K18-hACE2 +/- | Female | 2 | 6-10 | SARS-CoV-2(WA1/2020) | 1.0X 10 ⁴ / TCID 50 | 45 | Histology |
| C57BL/6J | Male | 3 | 6-8 | H1N1 A/PR/8/34 (PR8) | 50 PFU | 7 | Histology Staining |
| C57BL/6J | Male | 4 | 6-8 | H1N1 A/PR/8/34 (PR8) | 50 PFU | 14 | Histology Staining |
| C57BL/6J | Male | 5 | 6-8 | H1N1 A/PR/8/34 (PR8) | 50 PFU | 21 | Histology staining |
| K18-hACE2 +/- | Female | 4 | 8 | N/A | N/A | 0 | Bulk RNA seq |
| K18-hACE2 +/- | Female | 3 | 6-10 | SARS-CoV-2(WA1/2020) | 2.0X 10 ⁵ / TCID 50 | 4 | Bulk RNA seq |
| K18-hACE2 +/- | Female | 3 | 6-10 | SARS-CoV-2(WA1/2020) | 2.0X 10 ⁵ / TCID 50 | 6 | Bulk RNA seq |
| K18-hACE2 +/- | Female | 3 | 8-10 | H1N1 A/PR/8/34 (PR8) | 50 PFU | 4 | Bulk RNA seq |
| K18-hACE2 +/- | Female | 3 | 8-10 | H1N1 A/PR/8/34 (PR8) | 50 PFU | 6 | Bulk RNA seq |
| K18-hACE2 +/- | Female | 1 | 12 | SARS-CoV-2(WA1/2020) | 2.0X 10 ⁵ / TCID 50 | 4 | Single cell RNA seq |
| K18-hACE2 +/- | Female | 2 | 12 | H1N1 A/PR/8/34 (PR8) | 50 PFU | 4 | Single cell RNA seq |
| K18-hACE2 +/- | Female | 2 | 12 | H1N1 A/PR/8/34 (PR8) | 50 PFU | 6 | Single cell RNA seq |

DPI: Days post infection.

Supplemental Table 2. Statistically significant differentially expressed pathways between influenza and SARS-CoV-2-infected lungs at day 4 post infection.

| NAME | GS follow link to MSigDB | GS DET AILS | Set Size | ES | Normalized_Enrichment_Score | NO M p-val | FDR q-val | Pv al ue | RANK AT MAX | LEADING EDGE |
|------------------------------------|------------------------------------|-------------|----------|-----|-----------------------------|------------|-----------|----------|-------------|---------------------------------|
| HALLMARK_INTERFERON_GAMMA_RESPONSE | HALLMARK_INTERFERON_GAMMA_RESPONSE | Details ... | 15 | 0.6 | 3.912263 | 0 | 0 | 0 | 1218 | tags=75%, list=24%, signal=96% |
| HALLMARK_TNFRSF25_SIGNALING | HALLMARK_TNFRSF25_SIGNALING | Details ... | 14 | 0.6 | 3.768104 | 0 | 0 | 0 | 1144 | tags=68%, list=23%, signal=86% |
| HALLMARK_INFLAMMATORY_RESPONSE | HALLMARK_INFLAMMATORY_RESPONSE | Details ... | 13 | 0.6 | 3.589829 | 0 | 0 | 0 | 1190 | tags=69%, list=24%, signal=88% |
| HALLMARK_INTERFERON_ALPHA_RESPONSE | HALLMARK_INTERFERON_ALPHA_RESPONSE | Details ... | 86 | 0.6 | 3.470372 | 0 | 0 | 0 | 904 | tags=67%, list=18%, signal=81% |
| HALLMARK_IL6_JAK_STAT3_SIGNALING | HALLMARK_IL6_JAK_STAT3_SIGNALING | Details ... | 64 | 0.6 | 3.296526 | 0 | 0 | 0 | 506 | tags=56%, list=10%, signal=62% |
| HALLMARK_ALLOGRAFT_REJECTION | HALLMARK_ALLOGRAFT_REJECTION | Details ... | 11 | 0.5 | 3.239597 | 0 | 0 | 0 | 1189 | tags=64%, list=24%, signal=82% |
| HALLMARK_P53_PATHWAY | HALLMARK_P53_PATHWAY | Details ... | 95 | 0.4 | 2.692231 | 0 | 0 | 0 | 1203 | tags=54%, list=24%, signal=69% |
| HALLMARK_IL2_STAT5_SIGNALING | HALLMARK_IL2_STAT5_SIGNALING | Details ... | 10 | 0.4 | 2.389516 | 0 | 0 | 0 | 918 | tags=41%, list=18%, signal=49% |
| HALLMARK_COMPLEMENT | HALLMARK_COMPLEMENT | Details ... | 10 | 0.4 | 2.291471 | 0 | 1.43 E-04 | 0.0 | 1217 | tags=50%, list=24%, signal=65% |
| HALLMARK_KRAS_SIGNALING_UP | HALLMARK_KRAS_SIGNALING_UP | Details ... | 98 | 0.4 | 2.256511 | 0 | 1.29 E-04 | 0.0 | 891 | tags=38%, list=18%, signal=45% |
| HALLMARK_APOPTOSIS | HALLMARK_APOPTOSIS | Details ... | 80 | 0.4 | 2.158816 | 0 | 4.88 E-04 | 0.0 | 1387 | tags=52%, list=27%, signal=71% |
| HALLMARK_MYC_TARGETS_V2 | HALLMARK_MYC_TARGETS_V2 | Details ... | 30 | 0.4 | 2.103931 | 0 | 5.54 E-04 | 0.0 | 1896 | tags=87%, list=38%, signal=138% |
| HALLMARK_COAGULATION | HALLMARK_COAGULATION | Details ... | 60 | 0.4 | 2.067774 | 0 | 6.93 E-04 | 0.0 | 1395 | tags=53%, list=28%, signal=73% |

Supplemental Table 3. Statistically significant differentially expressed pathways between influenza and SARS-CoV-2-infected lungs at day 6 post infection

| NAME | GS follow link to MSigDB | GS DET AILS | S IZ E | ES | Normilized_ Enrichment_ Score | NO M p- val | FD R q- val | FWE R p- val | RANK AT MAX | LEADIN G EDGE |
|--|--|--------------|--------|------------|-------------------------------|-------------|-------------|--------------|-------------|---------------------------------|
| HALLMARK_TNFA_SIG NALING_VIA_NFKB | HALLMARK_TNFA_SIG NALING_VIA_NFKB | Detai ls ... | 1 0 6 | 0.6 062 44 | 3.1957 | 0 | 0 | 0 | 1332 | tags=83%, list=30%, signal=116% |
| HALLMARK_P53_PATH WAY | HALLMARK_P53_PATH WAY | Detai ls ... | 7 8 | 0.5 128 18 | 2.609483 | 0 | 0 | 0 | 1252 | tags=65%, list=28%, signal=89% |
| HALLMARK_KRAS_SIG NALING_UP | HALLMARK_KRAS_SIG NALING_UP | Detai ls ... | 8 9 | 0.4 976 07 | 2.554852 | 0 | 0 | 0 | 829 | tags=54%, list=19%, signal=65% |
| HALLMARK_EPITHELIAL_MESENCHYMAL_TRANSITION | HALLMARK_EPITHELIAL_MESENCHYMAL_TRANSITION | Detai ls ... | 7 7 | 0.4 725 35 | 2.381339 | 0 | 0 | 0 | 1375 | tags=66%, list=31%, signal=94% |
| HALLMARK_INFLAMMATORY_RESPONSE | HALLMARK_INFLAMMATORY_RESPONSE | Detai ls ... | 1 0 | 0.4 398 1 | 2.325041 | 0 | 0 | 0 | 756 | tags=49%, list=17%, signal=58% |
| HALLMARK_IL6_JAK_STAT3_SIGNALING | HALLMARK_IL6_JAK_STAT3_SIGNALING | Detai ls ... | 4 2 | 0.4 855 32 | 2.065453 | 0 | 0 | 0 | 1159 | tags=57%, list=26%, signal=77% |
| HALLMARK_TGF_BETA_SIGNALING | HALLMARK_TGF_BETA_SIGNALING | Detai ls ... | 2 4 | 0.4 868 25 | 1.854932 | 0.00 337 8 | 0.0 091 94 | 0.02 1 | 1539 | tags=79%, list=35%, signal=120% |
| HALLMARK_APOPTOSIS | HALLMARK_APOPTOSIS | Detai ls ... | 6 7 | 0.3 160 87 | 1.584815 | 0.01 442 3 | 0.0 733 86 | 0.17 2 | 826 | tags=42%, list=19%, signal=51% |
| HALLMARK_APICAL_JUNCTION | HALLMARK_APICAL_JUNCTION | Detai ls ... | 6 9 | 0.3 086 23 | 1.532568 | 0.00 934 6 | 0.0 926 13 | 0.23 1 | 776 | tags=32%, list=17%, signal=38% |
| HALLMARK_UV_RESPONSE_UP | HALLMARK_UV_RESPONSE_UP | Detai ls ... | 4 7 | 0.3 348 76 | 1.503433 | 0.03 589 7 | 0.1 050 78 | 0.27 6 | 1135 | tags=49%, list=25%, signal=65% |
| HALLMARK_COMPLEMENT | HALLMARK_COMPLEMENT | Detai ls ... | 7 7 | 0.2 751 05 | 1.387579 | 0.02 272 7 | 0.1 936 82 | 0.48 7 | 440 | tags=19%, list=10%, signal=21% |

Supplementary Table 4. Animal Information for Nonhuman Primate Comparators

| Species | Sex | Age | Weight | Inoculum | Timepoint |
|-----------------------------|------------|------------|---------------|-----------------|------------------|
| <i>Chlorocebus aethiops</i> | Male | 7.35 | 4.2 | RSV | 2 WPI |
| <i>Chlorocebus aethiops</i> | Male | 17.34 | 5.45 | SHAM | 4 WPI |
| <i>Chlorocebus aethiops</i> | Male | 16.33 | 7.45 | SARS-CoV-2 | 4 WPI |
| <i>Chlorocebus aethiops</i> | Male | 16.3 | 6.9 | SARS-CoV-2 | 4 WPI |
| <i>Chlorocebus aethiops</i> | Female | 16.29 | 3.85 | SARS-CoV-2 | 4 WPI |
| <i>Chlorocebus aethiops</i> | Female | 16.28 | 4.25 | SARS-CoV-2 | 2 WPI |

WPI: Weeks post SARS-CoV-2 infection.

Supplementary Table 5. Human Case Information

| Patient No. | 1 | 2 | 3 |
|-------------------------------------|--|---|--|
| Patient ID | UMAU20-00028 | TMC-20-1(A14-20-1) | TMC-21-3 |
| Age | 78 years | 58 years | 86 years |
| Gender | female | male | male |
| Comorbidities | end-stage renal disease, type 2 diabetes and obesity | hypertension, type 2 diabetes mellitus, hepatitis C virus and chronic kidney disease | bilateral sacral fracture, atrial fibrillation, heart failure, hypertension, hyperlipidemia, stage 3 chronic kidney disease, cerebrovascular disease, peripheral artery disease, esophageal dilation, Parkinson disease, benign prostatic hyperplasia, and smoking |
| duration after test positive | 2 day | 32 days | 17 days |
| histology changes | Her lungs exhibited early changes of COVID-19 disease and thrombosis. These included focal hemorrhage and severe alveolar edema with early hyaline membrane formation. She had numerous clots in the pulmonary vessels and severely elevated d-dimer levels (10,020 ng/ml; normal <250 ng/ml). The edema and hyaline membranes are early changes associated with diffuse alveolar damage. Case report can be found in [1]. | extensive acute bronchopneumonia with focal bacteria colonies of cocci, multifocal organizing pneumonia with predominantly fibrosing and focally fibrinous features, which were consistent with a background COVID-19 infection. Additional significant findings included hypertrophic cardiomegaly, severe calcific atherosclerosis of the coronary arteries, centrilobular and midzonal necrosis of the liver consist with severe ischemic necrosis, glomerulosclerosis and arteriosclerosis of the kidneys, and diffuse mediastinal, hilar and mesenteric reactive lymphadenopathy. Case report can be found in [1]. | aspiration pneumonia, emphysema, bone marrow, fat emboli, hypertensive hypertrophic cardiomyopathy, acute peritonitis, necrosis of the distal esophagus, glomerulosclerosis, and acute tubular necrosis. (Figures are attached as Supplemental Figure 10) |

| | | | |
|---|---|--|---|
| complications | cardiac arrest | end-stage renal failure requiring dialysis, and anoxic brain injury secondary to hypoxia | a right thigh hematoma and drop in hemoglobin, coffee ground emesis, pneumatosis of the stomach, pneumoperitoneum, necrosis of the distal esophagus, continued intraabdominal abscess, and bleeding from the spleen |
| progenitor cell staining description | Scattered krt-5 positive cells are found in SARS-CoV2 deposit area. No "pod" structure. | Scattered krt-5 positive cells are found in fibrosis area. No "pod" structure. | Very few krt-5 positive cells are found in fibrosis area. No "pod" structure. |

Reference:

1. Liu, F., et al., *SARS-CoV-2 Infects Endothelial Cells In Vivo and In Vitro*. *Front Cell Infect Microbiol*, 2021. **11**: p. 701278.

Supplementary Table 6. Antibody Information

| | | | | |
|--------------|---------------|---------|------------------------------|--------------|
| Anti-SARS | Anti-SARS-CoV | 1: 1000 | BEI Resources | # NR-10361 |
| Anti-CD206 | Anti-mouse | 1: 50 | R & D | # AF2535 |
| Anti-SMA | Anti-mouse | 1: 100 | Abcam | # ab5694-100 |
| Anti-Krt-5 | Anti-mouse | 1: 1000 | BioLegend | # 905901 |
| Anti-SMA | Anti-human | 1: 100 | Agilent | # M085129-2 |
| Anti-Krt-5 | Anti-human | 1: 50 | Abcam | # ab17130 |
| Anti-pro SPC | Anti-mouse | 1: 500 | Seven Hills Bioreagents | # WRAB-9337 |
| Anti-trp63 | Anti-mouse | 1: 200 | Cell Signaling Technology | # 13109 |
| Anti-NGFR | Anti-mouse | 1: 100 | Abcam | # ab52987 |